https://doi.org/10.31436/iiumej.v25i1.2811

THIOL FUNCTIONALIZED GOLD NANOBIPYRAMIDS-BASED PLASMONIC SENSOR FOR GLUCOSE DETECTION

NATASYA SALSABIILA[1,2,3], MARLIA MORSIN[1,2*], MUHAMMAD HANIF [1], SURATUN NAFISAH[1,2,3], NUR LIYANA RAZALI[1,2] AND IWANTONO[4]

[1]Faculty of Electrical & Electronic Engineering, Universiti Tun Hussein Onn Malaysia, 86400 Parit Raja, Batu Pahat, Johor, Malaysia
[2]Microelectronics & Nanotechnology - Shamsuddin Research Centre (MiNT-SRC), Institute of Integrated Engineering, Universiti Tun Hussein Onn Malaysia, 86400 Parit Raja, Batu Pahat Johor, Malaysia
[3]Department of Electrical Engineering, Faculty of Industrial and Production Technology, Institut Teknologi Sumatera (ITERA), Lampung Selatan, 35365 Indonesia
[4]Department of Physics, Faculty of Mathematics and Natural Sciences, Universitas Riau, Pekanbaru, 28293, Indonesia

[*]Corresponding author: marlia@uthm.edu.my

(Received: 30 March 2023; Accepted: 13 June 2023; Published on-line: 1 January 2024)

ABSTRACT: Gold nanobipyramids (GNBPs) have high selectivity in detecting changes in their surrounding medium because of their electric field enhancements and larger surface areas. In this study, we functionalized GNBPs using a thiol group that acts as a ligand to improve the detection performance of the analytes. The investigation is carried out by varying the functionalization periods from 12 to 72 hours. The optimum thiol-functionalized GNBPs (t-GNBPs) are obtained in 60 hours, with a length of 36.84 ± 2.05 nm, a width of 24.02 ± 0.74 nm, and an aspect ratio of 1.54 ± 0.11. Then, the optimum t-GNBPs are used as a sensing material in a plasmonic sensor to detect glucose. The limit of detection (LoD) of glucose is 1 µM for this sensor. The plasmonic sensor has been successfully built with reliable performance in detecting glucose with excellent linearity, sensitivity and R^2 = 1; good selectivity compared to four similar chemical structure analytes; high stability with a low error value, i.e., ± 0.02 a.u.; and almost consistent repeatability values in each cycle with low percent variance of 0.000025% for the t-SPR area and 0.000032% for the l-SPR area. Therefore, a plasmonic sensor based on t-GNBPs is an alternative method of detecting glucose with high sensitivity, selectivity and repeatability.

ABSTRAK: Nanobipiramid Emas (GNBPs) memiliki selektiviti yang tinggi dalam mengesan perubahan medium sekitar kerana memiliki peningkatan medan elektrik dan luas permukaan yang besar. Kajian ini merupakan fungsionalisasi terhadap GNBPs dengan menggunakan kumpulan thiol sebagai ligan bagi meningkatkan prestasi pengesanan analit. Kajian ini dilakukan dengan mempelbagaikan tempoh masa fungsionalisasi dalam julat waktu 12 hingga 72 jam. GNBPs optimum yang difungsionalisasi oleh thiol (t-GNBPs) diperoleh pada 60 jam, dengan panjang 36.84 ± 2.05 nm, lebar 24.02 ± 0.74 nm, dan nisbah aspek 1.54 ± 0.11. Kemudian, t-GNBPs optimum digunakan sebagai bahan penderia pada sensor plasmonik bagi mengesan glukosa. Limit pengesanan glukosa (LoD) bagi sensor ini adalah sebanyak 10^0 µM. Sensor plasmonik telah berhasil dibangunkan dengan kecekapan boleh percaya dalam mengesan glukosa dengan lineariti dan sensitiviti sebanyak R^2 = 1. Pemilihan yang baik dibandingkan dengan 4 analit yang sama dari segi struktur kimia. Kestabilan yang tinggi dengan nilai ralat rendah iaitu ± 0.02 a.u, dan memiliki nilai keberulangan yang hampir konsisten pada setiap kitar dengan peratusan varian rendah iaitu sebanyak 0.000025% bagi bahagian t-SPR dan 0.000032% bagi l-SPR. Oleh itu, pengesan plasmonik berdasarkan t-GNBPs ini adalah kaedah alternatif bagi mengesan glukosa dengan sensitiviti, selektiviti, dan kebolehulangan yang tinggi.

https://doi.org/10.31436/iiumej.v25i1.2811

KEYWORDS: *gold nanobipyramids; glucose; plasmonic sensor; thiol*

1. INTRODUCTION

Gold is a metal nanoparticle commonly used as a sensing material due to its unique surface plasmon resonance (SPR) property that makes it sensitive to the surrounding medium. In addition, this metal has high biocompatibility and reactivity, low cost, and is non-toxic and environmentally friendly [1]. The SPR properties of gold nanomaterials depend on their shape and size, with nanospherical being the most synthesized nanoparticles. Other than that, several forms of non-spherical gold nanoparticles have been successfully synthesized, such as nanorod, nanorice, nanoplate, and nanoarray, each of which can be used to detect mercury (II) and Hg^{2+} ions [2], boric acid [3], as well as sepsis [4]. Moreover, a form of non-spherical gold nanomaterial with high figures of merit is gold nanobipyramids (GNBPs), which has higher sensitivity and the potential to be applied as a sensing material in sensor systems [5]. The GNBPs have local field enhancements, a wider surface area than other forms, and a spectral surface that can be modified. The applications of GNBPs as sensing material include detecting glyphosate [5], aflatoxin B1 [6], and dopamine [7], using various detection methods. In this study, GNBPs have been synthesized and act as a sensing material for SPR-based sensors, called plasmonic sensors. The plasmonic sensor is chosen because it can detect analytes quickly and accurately.

The plasmonic sensor was built to detect glucose as a pre-indicator of diabetes. Diabetes is a type of disease in which the body is unable to produce insulin hormone properly, resulting in the body's inability to process carbohydrates into a source of energy, which is characterized by fluctuations in blood sugar from its normal range and can increase the prevalence of complications compared to other types of disease. According to the World Health Organization (WHO), diabetes is predicted to be the 7th most significant cause of death in 2030 [8]. According to a study conducted by Pouya et al., using the logistic regression method, it is predicted that people with diabetes worldwide will reach 578 million in 2030 and 700 million in 2045 [9]. Meanwhile, Malaysia was ranked 4th on the list of countries with the most diabetics in Southeast Asia in 2016. Then, Malaysia was also ranked as the 1st country with the highest number of people with diabetes in the West Pacific in 2018, with a prevalence reaching 16.8% and affecting 3.6 million people from the total adult population. Also, the annual costs incurred by Malaysia reached US$ 600 million [10]. Thus, it is crucial to have the glucose detection system to improve diabetes care and the plasmonic sensor is an alternative method to solve this problem.

Functionalization was performed on the GNBPs surface to produce additional ligands that bind with the targeted analyte. Thiol, as one of the functionalization agents, is commonly used for detecting glucose due to its ability to conjugate with strong affinity on the nanoparticle surface. Therefore, it can bind with carbohydrate molecules such as glucose and increase the sensor's selectivity, characterized by long emission waves [11]. Thus far, several researchers have reported that thiol can be used in gold nanoparticles to detect glucose. A study by Samanta *et al.* performed glucose detection based on gold nanospheres [12]. Then, a study by Asim *et al.* used thiol to functionalize thin gold film as a sensing material [13]. Another structure is cubes functionalized with thiol, used in the study by Zhenyu et al. with an electrochemical detection method [14]. Meanwhile, GNBPs have shown a promising and greater potential structure to be functionalized with thiol and used to detect glucose as well due to their several advantages, i.e., the higher figure of merit value compared to other structures. Hence, this study proposes thiol-functionalized GNBPs (t-GNBPs) as a sensing material for detecting glucose based on plasmonic resonance.

https://doi.org/10.31436/iiumej.v25i1.2811

2. MATERIALS AND METHOD

2.1 Materials

The materials used in this study were gold (III) chloride trihydrate ($HAuCl_4.3H_2O$), chloroplatinic acid hydrate ($H_2PtCl_4.H_2O$), cetylmethylammonium bromide ($C_{19}H_{42}BrN$), sodium borohydride ($NaBH_4$), ascorbic acid ($C_6H_8O_6$), and (3-mercaptoropyl) trimethoxysilane which were purchased from Sigma Aldrich, USA. Silver nitrate ($AgNO_3$) and hydrochloric acid (HCl) were purchased from RCI Labscan.

2.2 Preparation of Gold Nanobipyramids

2.2.1 Synthesis

The synthesis method used was the bottom-up seed-mediated growth method (SMGM) which is divided into two processes, i.e., seeding and growth, as mentioned in the previous studies [5]. The materials needed to produce bipyramid nanoseeds solution include $HAuCl_4.3H_2O$ (0.15, 0.01 M), $H_2PtCl_4.H_2O$ (0.1 mL, 0.01 M), $C_{19}H_{42}BrN$ (9.75 mL, 0.1 M), and cold $NaBH_4$ (0.9 mL, 0.01 M), which were mixed and then left undisturbed for 2 hours at 27 ºC. After 2 hours, the nanoseeds were used for the growth process. The materials needed to produce growth solutions include $HAuCl_4.3H_2O$ (0.875 mL, 0.01 M), $H_2PtCl_4.H_2O$ (0.0025 mL, 0.01 M), $C_{19}H_{42}BrN$ (20 mL, 0.1 M), $AgNO_3$ (0.2 mL, 0.01 M), HCl (0.4 mL, 1 M), $C_6H_8O_6$ (0.16 mL, 0.1 M), and 0.05 mL of nanoseeds. The materials were mixed and left undisturbed for 2 hours at 27 ºC. After 2 hours, the growth solution was functionalized with thiol groups.

2.2.2 Functionalization

The thiol group (3-mercaptopropyl) trimethoxysilane was diluted in 20 mL ethanol (10 mM) for the functionalization solution. Then, 2 mL of functionalization solution was added to the growth solution and stirred at 500 rpm with several time variations. The time variations in the stirring process included 12 hours, 24 hours, 48 hours, 60 hours, and 72 hours. Meanwhile, the temperature during the stirring process was kept constant at 27 ºC.

2.2.3 Characterization

In this work, the characterization was carried out using ultraviolet - visible (UV - Vis), X-Ray Diffraction (XRD), and Field Emission Scanning Electron Microscopy (FESEM). Each technique was used to observe the optical, structural, and morphological properties of t-GNBPs. For UV-Vis characterization, the UV-1800 Shimadzu Spectrophotometer (Japan) instrument was used with a wavelength range of 400 nm – 1000 nm. The XRD characterization uses the Bruker D8 Advance X-Ray Diffractometer (Germany) device with an angle range of 20º - 60º. Meanwhile, the FESEM characterization uses the Joel JSM-7600 Field Emission Scanning Electron Microscopy (USA) instrument. The characterization samples were centrifuged for 30 minutes at 5000 rpm and then dispersed in a deionized water (DIW) solution. This process was repeated three times. After that, the residue was mixed with 25 µL DIW and deposited on glass and ITO substrates for XRD and FESEM characterization, respectively. Finally, the sample substrate was dried in an oven for 30 minutes at 50 ºC.

2.3 Preparation of Analytes

The glucose target analyte (20 mL) was prepared with various concentrations, including 10^0 µM, 10^1 µM, 10^2 µM, 10^3 µM, 10^4 µM, 10^5 µM, and 10^6 µM. This variation was selected to improve the range of glucose levels in an automatic insulin delivery system with adjustable glucose in a previous study, i.e., 110 mg/dL – 150 mg/dL (6111.1 µM – 8333.3 µM) [15]. For

https://doi.org/10.31436/iiumej.v25i1.2811

the selectivity study, lactose, natrium, vitamin C, and calcium were used as analytes, each was prepared in 20 mL with a concentration of 10^1 µM.

2.4 Plasmonic Sensor Setup

The plasmonic sensor comprises six components: a light source, simplex fiber optic, chamber, material sensing, and a computer equipped with Ocean View Software to analyze the absorbance spectrum data. The component setup used is shown in Fig. 1. This component setup refers to previous research on herbicide detection using gold nanorods [16]. In contrast, for detecting formaldehyde, boric acid, and glyphosate, the duplex fiber optic type was used to have a different setup [5].

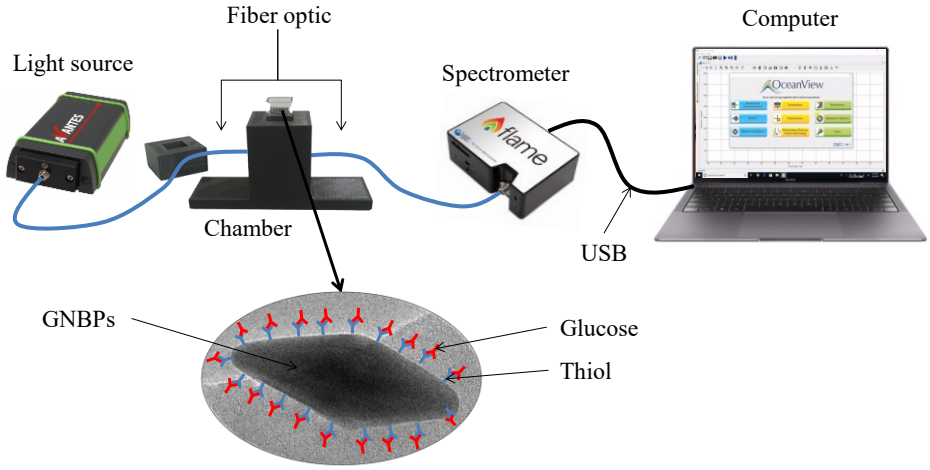

Fig. 1: The setup of the plasmonic sensor for glucose detection.

3. RESULTS AND DISCUSSION

3.1 Synthesis of GNBPs

GNBPs were successfully synthesized using the SMGM method. The initial observation was made by analyzing the color change in the solution during the synthesis process. After successful seeding, the nanoseeds solution turned brown, as shown in Fig. 2(a). This color is consistent with previous research [17], which said that a color change indicates a nanoseeds size of 4 nm. Meanwhile, the solution changed color to purple for the growth process, as shown in Fig. 2(b), which appeared during the first 30 minutes of reaction time. In this process, $C_{19}H_{42}BrN$ functions as a capping agent which controls the elongation of gold particles. Then, adding $AgNO_3$ affects the formation of GNBPs during the growth process.

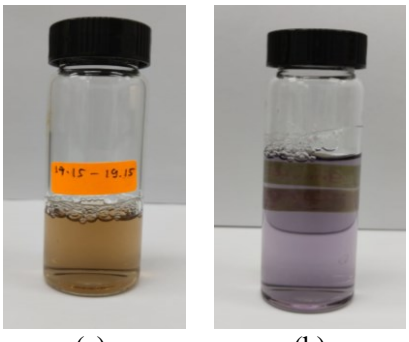

(a) (b)

Fig. 2: Color visualization of (a) nanoseeds solution and (b) growth solution.

https://doi.org/10.31436/iiumej.v25i1.2811

3.2 Effect of Thiol Functionalization on GNBPs

Functionalization of GNBPs using thiol was successfully carried out after the growth solution was produced. The solution was prepared using 12- to 72-hour time variations to determine the optimum and specific functionalization time. After the stirring process with a magnetic stirrer, the resulting t-GNBPs solution is shown in Fig. 3. The solution's color changed from dark purple to light purple as the functionalization time increased. Thus, it can be confirmed that t-GNBPs were successfully formed. As a comparison, an unfunctionalized solution was also observed and denoted as 0 hours.

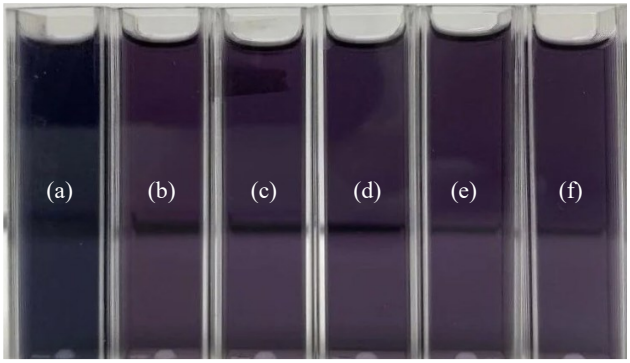

Fig. 3: Final color solution after functionalization with (a) 0 hours, (b) 12 hours, (c) 24 hours, (d) 48 hours, (e) 60 hours, and (f) 72 hours.

Optical characterization was carried out using UV-Vis. The resulting absorbance spectrum is shown in Fig. 4. The figure shows the spectral region in the range of 400 – 1000 nm and has two peaks, namely Transverse Surface Plasmon Resonance (t-SPR) in the area of 500 nm – 600 nm and Longitudinal Surface Plasmon Resonance (l-SPR) in the range of 700 nm – 900 nm. The intensity and peak positions of the absorbance spectrum are formulated in Table 1. Based on the data in Fig. 4 and Table 2, it was found that the absorbance spectrum underwent a hyperchromic shift in the range of 0 hours – 60 hours. In contrast, the hypochromic change occurred in the range of 60 hours – 72 hours. Thus, t-GNBPs with a functionalization time of 60 hours are the optimum sample, also used as a sensing material in a plasmonic sensor.

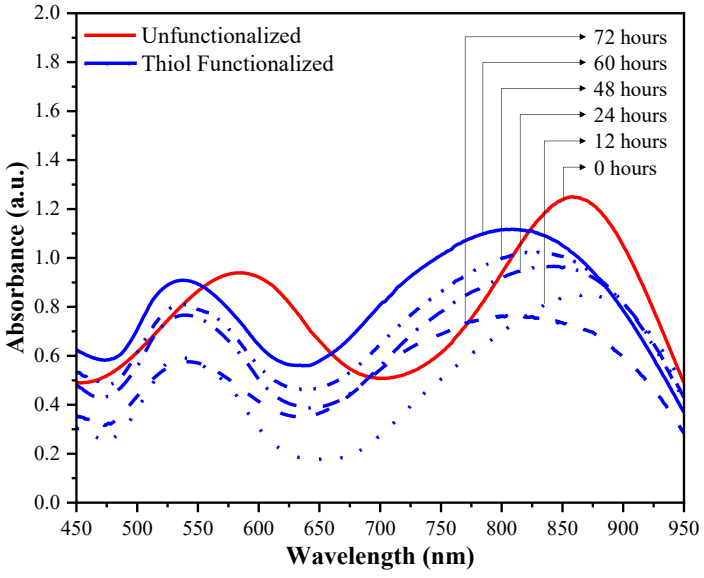

Fig. 4: The UV-Vis Spectrum of t-GNBPs.

https://doi.org/10.31436/iiumej.v25i1.2811

Table 1: Position of the peak wavelength and absorbance of t-GNBPs in the t-SPR and l-SPR areas

Sample (hours)	t-SPR		l-SPR	
	λ (nm)	I (a.u.)	λ (nm)	I (a.u.)
0	586	0.942	855	1.249
12	536	0.606	874	0.851
24	540	0.735	843	0.966
48	542	0.791	830	1.024
60	544	0.881	810	1.117
72	559	0.551	804	0.764

XRD was used for structural characterization to determine the chemical and crystal structure composition of the t-GNBPs, as shown in Fig. 5. The figure shows six samples and their detailed diffraction peak positions are detailed in Table 2. Each sample shows two diffraction peaks in the range of 20º - 60º. The positions of the two peaks follow the standard Inorganic Crystal Structure Database (ICSD) file No. 98-061-1625, with the resulting gold particles having a face-centered cubic (FCC) crystal structure. The crystal size of t-GNBPs was calculated using the Debye-Scherrer equation. The highest peak was obtained in the (111) plane at 38.105º – 38.369º, indicating that the dominant preferred orientation of the crystal is parallel to the surface of the substrate. Another FCC gold nanocrystal was found in the (200) plane at 44.458º – 44.555º. In general, the functionalization process slowly increased the intensity of the (111) and (200) planes compared to pure GNBPs.

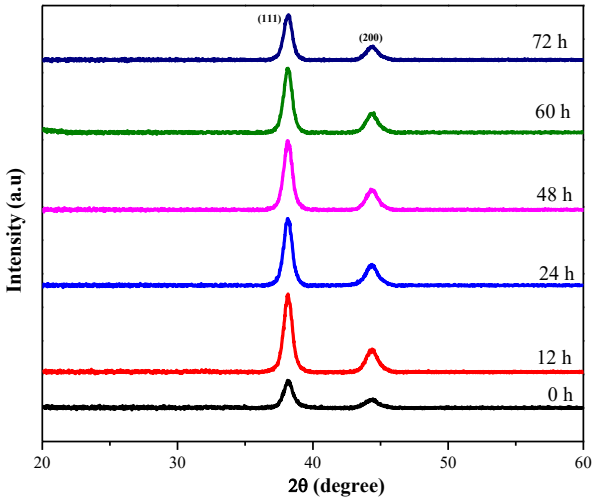

Fig. 5: XRD pattern of t-GNBPs.

Table 2: Detailed of t-GNBPs XRD parameters

Sample (hours)	Plane (111)		Plane (200)		FWHM	Crystallite Size (nm)
	2θ (º)	I (a.u)	2θ (º)	I (a.u.)		
0	38.152	770.58	44.554	218.26	0.354	23.731
12	38.369	1843.39	44.555	598.25	0.197	42.739
24	38.212	1949.62	44.458	567.93	0.433	19.416
48	38.294	1856.23	44.313	583.42	0.240	35.038
60	38.108	1878.87	44.302	556.83	0.624	13.468
72	38.239	1299.21	44.398	378.29	0.720	11.678

https://doi.org/10.31436/iiumej.v25i1.2811

Subsequently, morphological characterization was performed using FESEM, as shown in Fig. 6, to confirm the shape. Then, the aspect ratio and surface density analysis were performed. The aspect ratio is the ratio between the length and width of the nanomaterial. Meanwhile, the surface density is the ratio between the area covered by t-GNBPs and the entire area [16]. The analysis and calculations were done using ImageJ Software, as shown in Table 3. Based on the data in Table 3, it was found that an increase in functionalization time has caused a decrease in surface density, length, width, and aspect ratio in general. The resulting truncated t-GNBPs (by-products) continued to increase along with the increase in functionalization time because as the functionalization time rose, the gold source decreased, causing some nanoseeds to have insufficient gold sources to grow as perfect GNBPs. The surface density directly correlates with the resulting LSPR phenomenon and sensor sensitivity [18]. Decreases in the length, width, and surface density have caused a reduction in the peak of the absorbance spectrum, a spectral shift towards blue (blue shift), and reduced sensitivity. In addition, increasing functionalization time affected the bipyramidal shape, which became spherical-like. This is because the excess functionalization agents or molecules can etch the nanobipyramids' surfaces and remove material from the sharp tips and edges of the bipyramids, leading to a more rounded shape. Moreover, the Ostwald ripening process can also occur, where smaller nanobipyramids dissolve and transfer material to larger particles, resulting in a more uniform and spherical morphology [19]. Therefore, the functionalization process has allowed a morphological change.

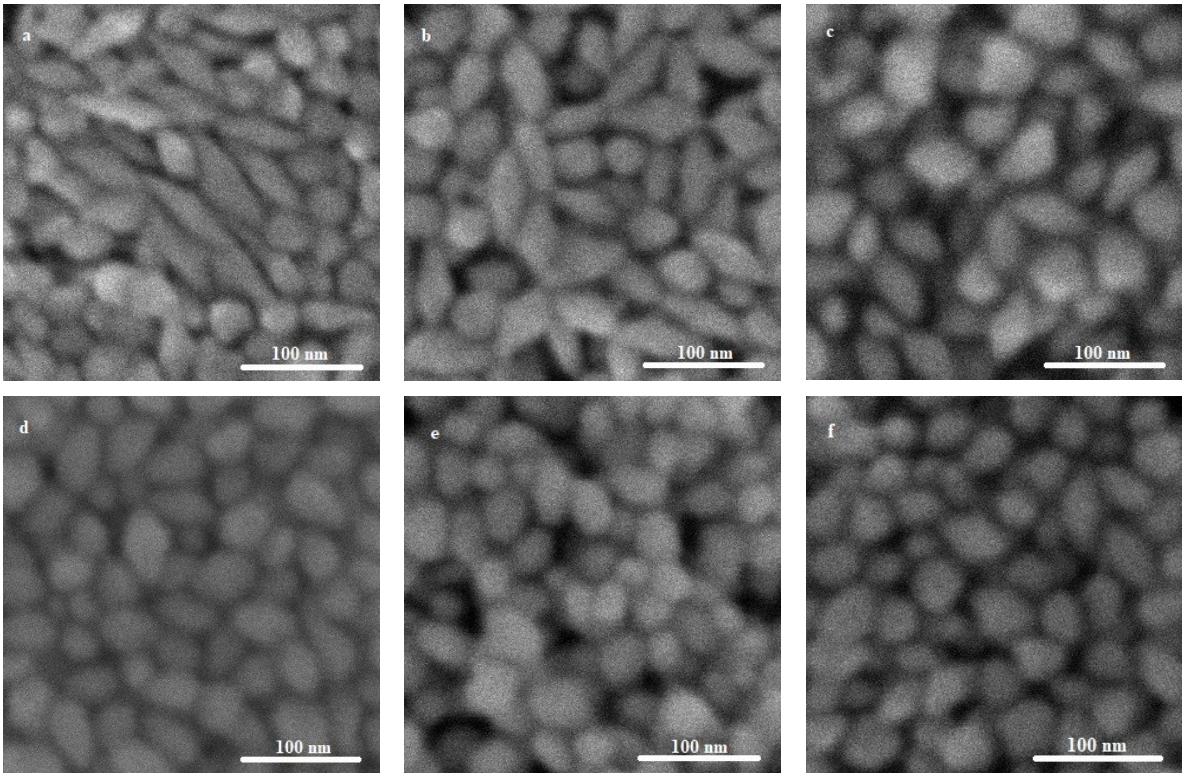

Fig. 6: FESEM image of t-GNBPs synthesized with a variation of time (a) 0 hours, (b) 12 hours, (c) 24 hours, (d) 48 hours, (e) 60 hours, and (f) 72 hours.

https://doi.org/10.31436/iiumej.v25i1.2811

Table 3: Length, width, and aspect ratio of sampled t-GNBPs and truncated t-GNBPs

Sample (hours)	Average Size							
	t-GNBPs				Truncated t-GNBPs			
	Surface Density (%)	Width (nm)	Length (nm)	Aspect Ratio	Surface Density (%)	Width (nm)	Length (nm)	Aspect Ratio
0	19.08±6.09	31.31±8.33	59.37±2.97	2.09±0.37	7.08±0.32	27.10±0.34	22.72±0.92	1.04±0.03
12	15.03±1.92	27.85±0.99	53.81±5.85	1.93±0.20	9.40±0.83	33.05±1.71	28.39±1.53	1.17±0.06
24	11.53±1.13	25.86±0.75	44.58±4.15	1.73±0.16	7.88±0.58	27.02±1.04	29.10±1.06	1.08±0.00
48	11.21±0.67	25.57±0.58	43.80±1.84	1.71±0.05	7.19±0.89	27.00±0.98	26.49±2.30	0.98±0.92
60	8.84±5.32	24.02±0.74	36.84±2.05	1.54±0.11	5.17±0.57	23.02±1.08	22.33±1.46	1.03±0.02
72	0.70±0.12	5.47±0.85	13.25±2.25	2.66±0.85	0.50±0.06	7.39±1.44	7.10±0.60	1.09±0.28

3.3 t-GNBPs as a Sensing Material for Glucose Detection

3.3.1 Plasmonic Response

A plasmonic response test was performed to ensure that t-GNBPs can detect glucose. The system was observed in two mediums, DIW as a reference and glucose 10^1 µM as the target analyte. The test results are shown in Fig. 7.

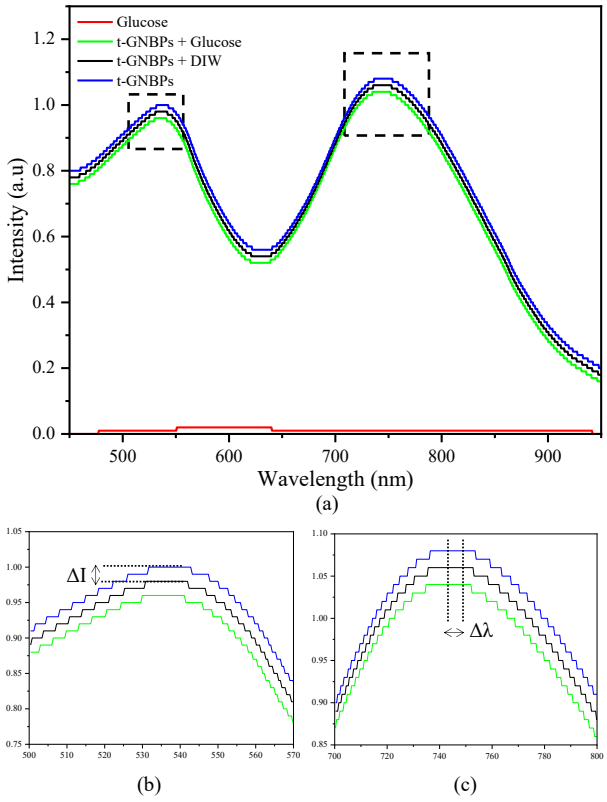

Fig. 7: (a) The plasmonic response of t-GNBPs spectrum. DIW and glucose medium show (b) intensity change and (c) wavelength shift.

Pure 10^1 µM glucose was also recorded by the plasmonic sensor system for comparison. The results show that pure 10^1 µM glucose does not have any peak, proving that the LSPR response generated by the plasmonic sensor is caused by t-GNBPs as material sensing. The positions of the peak intensity and wavelength of the system response are shown in Table 4.

https://doi.org/10.31436/iiumej.v25i1.2811

Furthermore, t-GNBPs with various functionalization times were tested in the DIW and 10^1 µM glucose medium, shown in Fig. 8 and Fig. 9, respectively. The precise peak position for each medium is shown in Table 5 and Table 6. It can be confirmed that 60 hours was an optimum functionalized time through its highest intensity spectrum compared to others in DIW and glucose medium. Then, t-GNBPs with 60 hours of functionalization time were used as sensing material to detect glucose and tested for sensor performances, namely sensitivity, selectivity, stability, and repeatability.

Table 4: Sensor response using t-GNBPs in DIW and glucose

Medium	t-SPR		l-SPR	
	λ (nm)	I (a.u)	λ (nm)	I (a.u.)
Pure t-GNBPs	537.244	1.00	744.804	1.08
DIW	536.391	0.98	744.010	1.06
Glucose	535.539	0.96	743.215	1.04

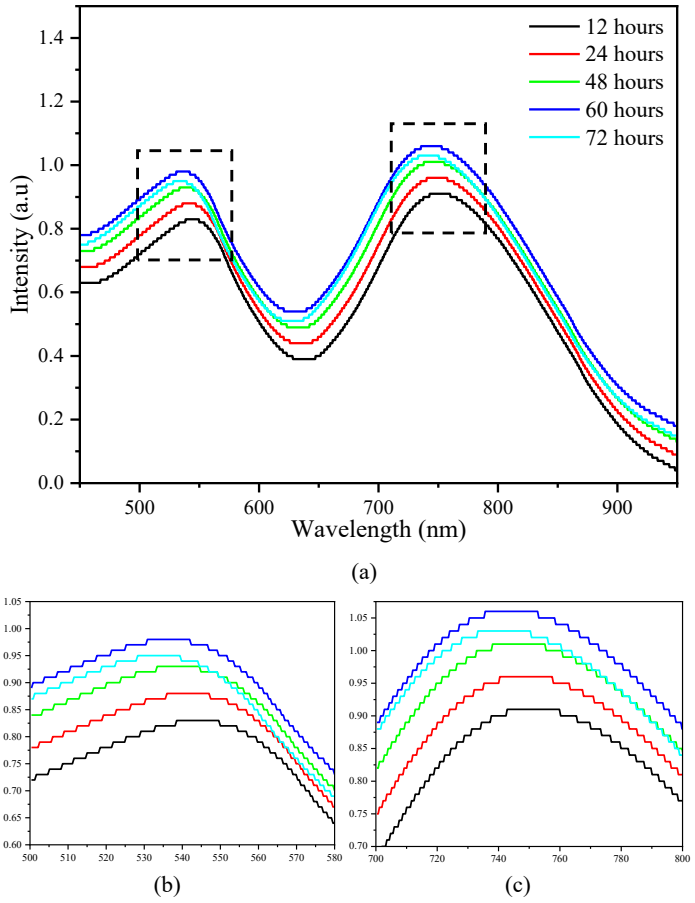

Fig. 8: (a) The plasmonic response of t-GNBPs in DIW medium, with (b) t-SPR area and (c) l-SPR area.

3.3.2 Sensitivity Test

The sensitivity test used two test parameters, peak intensity and wavelength changes, referring to previous studies [5]. This test was conducted to determine the effect of t-GNBPs as a sensing material on the resulting sensor response. In this test, the medium used was glucose

with several concentration variations, i.e., 10^0 µM, 10^1 µM, 10^2 µM, 10^3 µM, 10^4 µM, 10^5 µM, and 10^6 µM. The resulting sensor response is shown in Fig. 10. Meanwhile, the peak intensity and wavelength positions are shown in Table 7.

Table 5: The exact peak position of t-GNBPs in DIW medium

Medium	t-SPR		l-SPR	
	λ (nm)	I (a.u)	λ (nm)	I (a.u.)
12	544.056	0.83	751.150	0.91
24	541.503	0.88	748.770	0.96
48	538.948	0.93	746.390	1.01
60	536.391	0.98	744.010	1.06
72	533.832	0.95	741.625	1.03

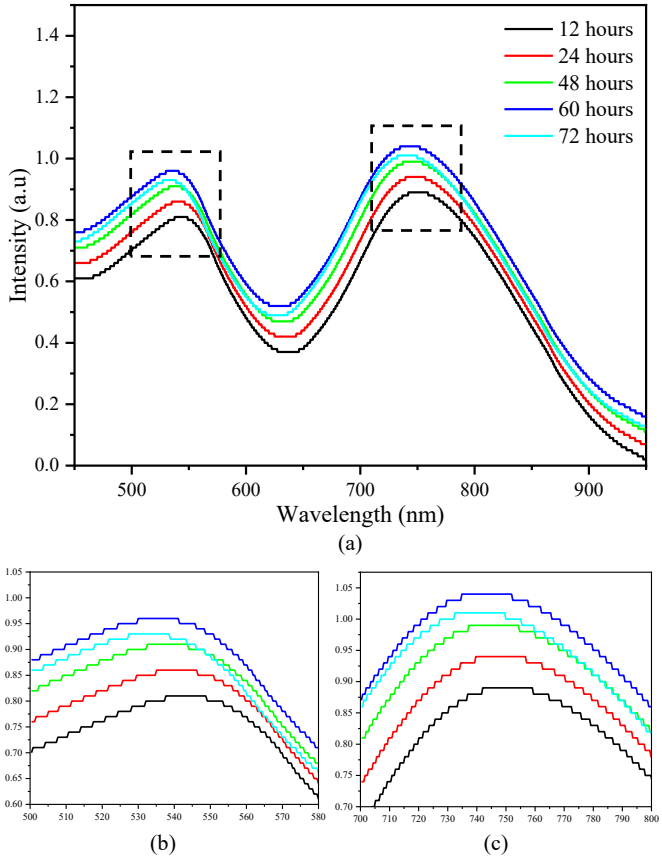

Fig. 9: (a) The plasmonic response of t-GNBPs in glucose medium, with (b) t-SPR area and (c) l-SPR area.

Table 6: The precise peak position of t-GNBPs in glucose medium

Medium	t-SPR		l-SPR	
	λ (nm)	I (a.u)	λ (nm)	I (a.u.)
12	543.205	0.81	750.360	0.89
24	540.651	0.86	747.980	0.94
48	538.096	0.92	745.599	0.99
60	535.539	0.96	743.215	1.04
72	532.979	0.93	740.829	1.01

https://doi.org/10.31436/iiumej.v25i1.2811

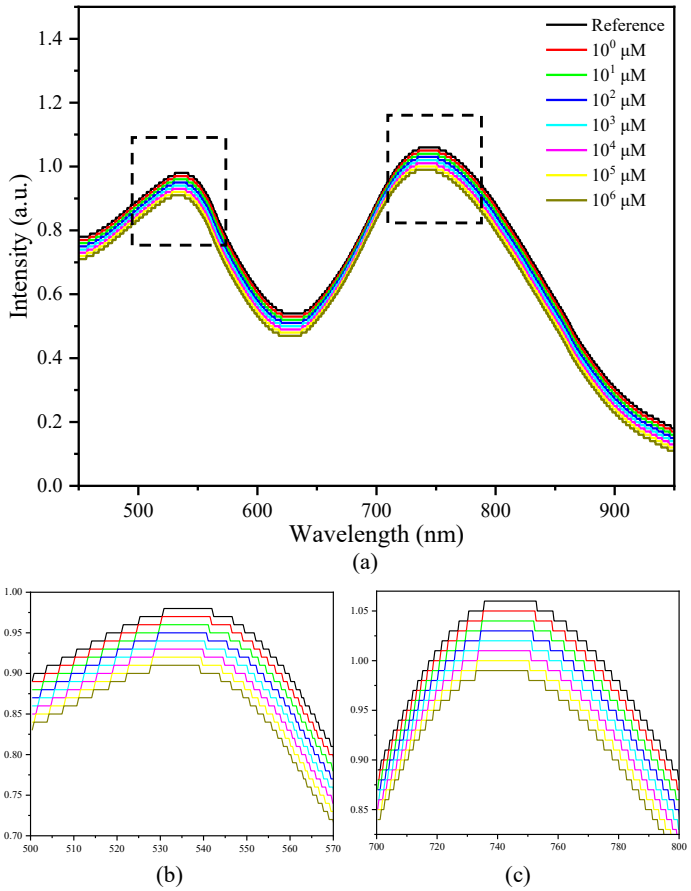

Fig. 10: (a) System response using t-GNBPs. DIW and glucose concentration variations show intensity and wavelength shifts in (b) t-SPR and (c) l-SPR.

Table 7: The detailed peak intensity and wavelength position in system response.

Glucose Concentration (µM)	t-SPR		l-SPR	
	λ (nm)	I (a.u)	λ (nm)	I (a.u.)
0	536.391	0.98	744.010	1.06
10^0	535.965	0.97	743.613	1.05
10^1	535.539	0.96	743.215	1.04
10^2	535.112	0.95	742.818	1.03
10^3	534.686	0.94	742.420	1.02
10^4	534.259	0.93	742.023	1.01
10^5	533.832	0.92	741.625	1.00
10^6	533.406	0.91	741.227	0.99

Based on Fig. 10 and Table 7, it was found that an increase in glucose concentration caused a constant decrease in peak intensity of 0.01 a.u. In the t-SPR region, the peak intensity decreased from 0.98 a.u. to 0.91 a.u., while in the l-SPR area, it occurred from 1.06 a.u. to 0.99 a.u. The decrease in wavelength and an increase in glucose concentration caused the absorbance spectrum to shift towards the blue region and it occurred constantly. In the t-SPR region, the shift in wavelength started from 536.391 nm to 533.406 nm, while in the l-SPR region, it appeared from 744.010 nm to 741.227 nm. Thus, t-GNBPs can be used as a sensing material to detect glucose in the range of 10^0 µM, 10^1 µM, 10^2 µM, 10^3 µM, 10^4 µM, 10^5 µM,

https://doi.org/10.31436/iiumej.v25i1.2811

and 10^6 µM, or equal to 0.000198 mg/mL – 198.17 mg/mL. Then, the changes in glucose concentration to changes in peak intensity and wavelength are shown in Fig. 11 and Fig. 12, respectively.

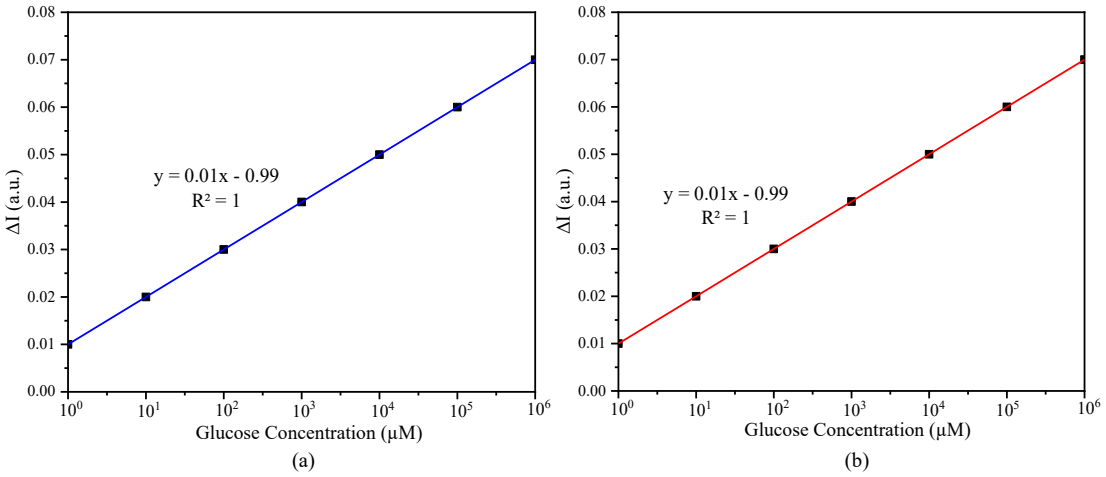

Fig. 11: Linearity between glucose concentration and peak intensity changes in (a) t-SPR and (b) l-SPR region.

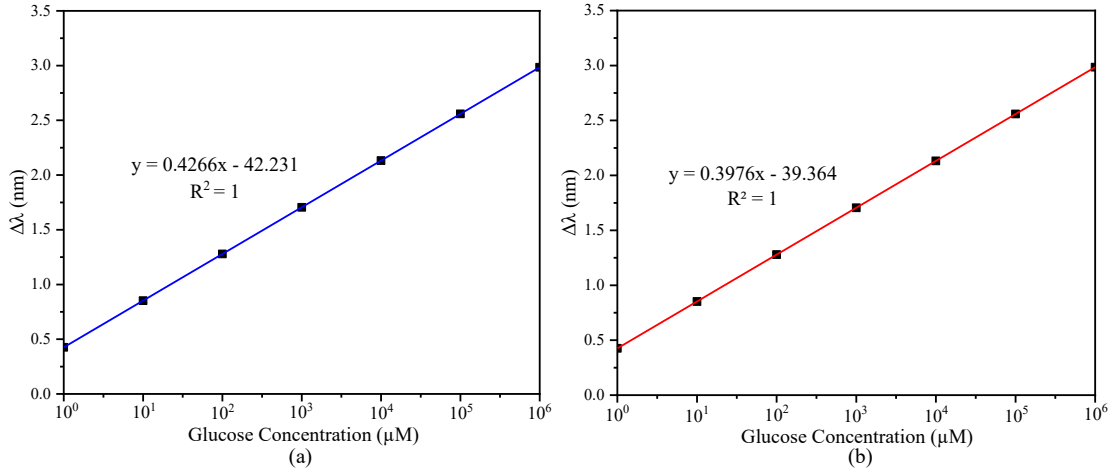

Fig. 12: Linearity between glucose concentration and wavelength shift in (a) t-SPR and (b) l-SPR region.

Figures 11 and 12 show that t-GNBPs have excellent linearity with an R^2 value of 1 at peak intensity and wavelength changes. For changes in peak intensity, the resulting linear regression was 0.01x – 0.99 in both the t-SPR and l-SPR regions. As for the shift in wavelength, the resulting linear regression was 0.4266x – 42.231 for the t-SPR region and 0.3976x – 39.364 for the l-SPR region. This equation can determine unknown glucose concentrations in further research and development. The positions of changes in intensity and wavelength peaks are shown in Table 8. Based on the data, the highest intensity peak changes occurred in 10^6 µM glucose medium of 0.07 a.u. Meanwhile, the highest change in wavelength also happened in the same medium of 2.985 nm for the t-SPR region and 2.783 nm for the l-SPR region.

The linearity generated by the t-GNBPs-based plasmonic sensor indicates that the blue shift of the spectral peaks occurred proportionally and constantly with increasing glucose concentration. Good linearity is a prominent indicator of sensor performance and indicates that

https://doi.org/10.31436/iiumej.v25i1.2811

the detected glucose concentration is stable. In addition, good linearity is also in line with good sensitivity, as evidenced by the steep slope of the graph. The steeper resulting graph indicates that the change in the value of the sensor output is also increasing in response to small input changes from analytes [20]. Thus, the plasmonic sensor has good performance and can be used to detect glucose properly.

Table 8: The detailed peak intensity and wavelength position in system response.

Glucose Concentration (μM)	t-SPR		l-SPR	
	λ (nm)	I (a.u)	λ (nm)	I (a.u.)
10^0	0.426	0.01	0.397	0.01
10^1	0.852	0.02	0.795	0.02
10^2	1.279	0.03	1.192	0.03
10^3	1.705	0.04	1.590	0.04
10^4	2.132	0.05	1.987	0.05
10^5	2.559	0.06	2.385	0.06
10^6	2.985	0.07	2.783	0.07

3.3.3 Selectivity Test

This test was conducted to assess the ability of the plasmonic sensor to detect sugar analytes such as glucose and lactose and non-sugars such as natrium, vitamin C, and calcium. Each analyte used in the test has a concentration of 10^1 μM to avoid value saturation. Prior to the test, pure GNBPs had been compared with GNBPs with thiol functionalization and it appears that the functionalized GNBPs have higher selectivity. Lactose was chosen because it has a chemical structure similar to glucose, i.e., $C_{12}H_{22}O_{11}$ for lactose and $C_6H_{12}O_{11}$ for glucose. While the selection of natrium, vitamin C, and calcium was made because both are substances that are often found in the blood and act as indicators of disease, such as natrium as an indicator of hypertension, vitamin C as an indicator of nutritional deficiency disease, and calcium as an indicator of human bone health. The selection of this analyte also refers to previous studies [21]. The resulting sensor response is shown in Fig. 13(b).

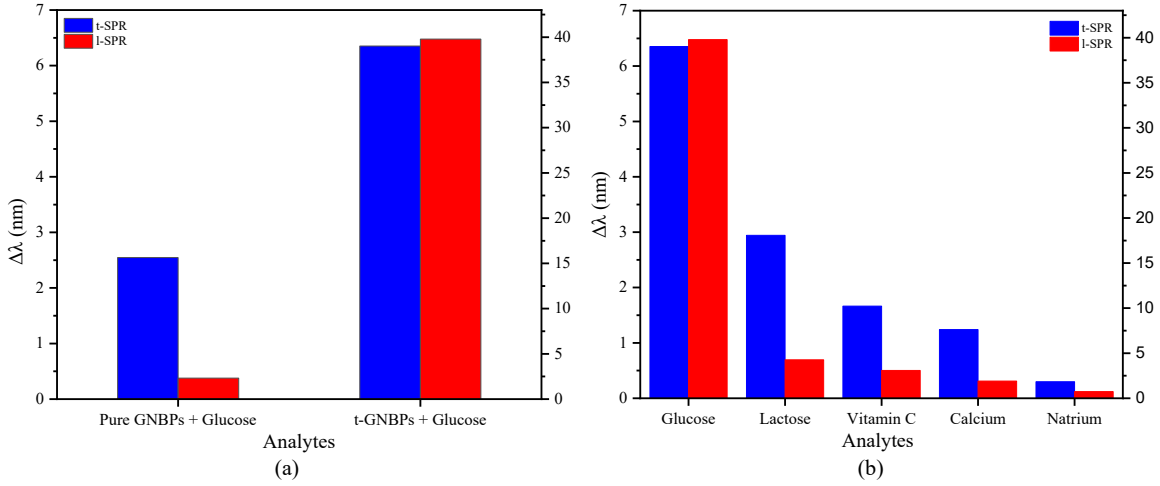

Fig. 13: The selectivity response of the plasmonic sensor in (a) pure GNBPs and functionalized GNBPs (b) five different analytes.

https://doi.org/10.31436/iiumej.v25i1.2811

Figure 13 shows that the plasmonic sensor is selective in detecting glucose, with the parameters used being changes in wavelength referring to previous studies [5]. The l-SPR region has a higher wavelength change value indicating that this region is more sensitive to changes in substituents and analytes. Lactose and vitamin C have high values because they have a chemical structure similar to glucose. Thus, plasmonic sensors based on t-GNBPs can detect glucose and non-glucose even though they have almost the same chemical structure.

3.3.4 Stability Test

t-GNBPs were tested in DIW medium and 10^1 µM for 10 minutes without stopping to test the stability of the plasmonic sensor. For sensor testing, the response was located at a wavelength of 536.391 nm for the t-SPR region and 535.539 nm for the l-SPR region. Fig. 14 shows the stability response using t-GNBPs as a sensing material for the t-SPR and l-SPR regions. In the t-SPR area, the average intensity value was 0.9789 ± 0.002 a.u. for DIW and 0.9600 ± 0.02 a.u. for glucose. While in the l-SPR area, the average intensity value was 1.0609 ± 0.02 a.u. for DIW and 1.0399 ± 0.02 a.u. for glucose. The relatively low error values indicate that the plasmonic sensor has high resistance to use for 10 minutes non-stop.

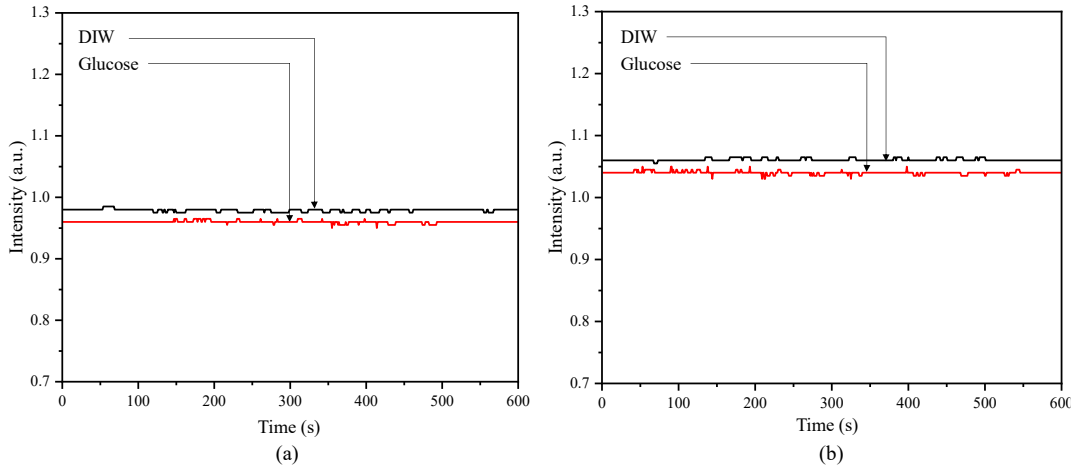

Fig. 14: The stability response of the plasmonic sensor for t-GNBPs in (a) t-SPR and (b) l-SPR peaks.

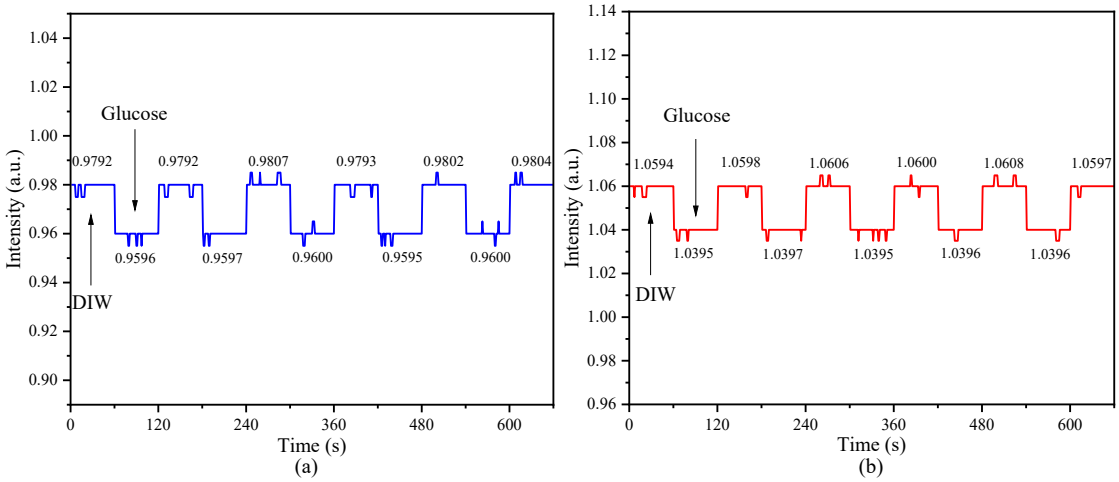

Fig. 15: The stability response of the plasmonic sensor for t-GNBPs in (a) t-SPR and (b) l-SPR region.

3.3.5 Repeatability Test

The repeatability test was carried out using DIW medium and glucose 10^1 µM every 60 seconds with five cycles of repetition for each peak, as shown in Fig. 15. Based on this figure, the average intensity of the t-SPR region for DIW and glucose was 0.9797 a.u. and 0.9598 a.u., respectively, with the difference between the two being 0.0199 ± 0.0001. Then in the l-SPR area, the average intensity for DIW and glucose was 1.0601 a.u. and 1.0396 a.u., with the difference between the two being 0.0205 ± 0.0005. The percent of variance for 5 iteration cycles was 0.000025% for the t-SPR area and 0.000032% for the l-SPR area. The low value of the iteration variance indicates that the plasmonic sensor based on t-GNBPs has excellent performance in detecting glucose.

4. CONCLUSION

GNBPs were successfully synthesized using the SMGM method. The functionalization process using thiol groups was done using several time variations from 12 – 72 hours. The optimum functionalization time was 60 hours, producing t-GNBPs in a length of 36.84 ± 2.05 nm, a width of 24.02 ± 0.74 nm, and an aspect ratio of 1.54 ± 0.11. In addition, an increase in functionalization time caused a decrease in t-GNBPs and an increase in truncated t-GNBPs. For this reason, it is necessary to continue this study on the functionalization time below 12 hours to determine the appropriate time for the t-GNBPs to grow ideally. The functionalization time also has affected the resulting sensor sensitivity response, which constantly decreased and shifted towards the blue spectrum as the glucose concentration increases. However, this system has excellent linearity and selectivity for glucose and non-glucose analytes. In addition, this system also has high stability with a low error value of ± 0.02 a.u. for 10 minutes. Besides that, the system has a low percent variance of 0.000025% for the t-SPR area and 0.000032% for the l-SPR area, resulting in a good performance in detecting glucose.

ACKNOWLEDGEMENT

The authors would like to thank Direktorat Riset, Teknologi, dan Pengabdian kepada Masyarakat (DRTPM) Ministry of Education, Culture, Research, and Technology Indonesia for supporting the project under PDUPT Research Grant (Contract No. 2595/UN19.5.1.3/PT.01.03/2022) and Universiti Tun Hussein Onn Malaysia through International Grant No. W024. Extended gratitude is expressed to Microelectronics & Nanotechnology - Shamsuddin Research Centre (MiNT-SRC) for the laboratory facilities.

REFERENCES

[1] Sani A, Cao C, Cui D. (2021) Toxicity of gold nanoparticles (AuNPs): A review. Biochem. Biophys. Reports, 26: 100991. doi: 10.1016/j.bbrep.2021.100991

[2] Zhang W, Liu G, Bi J, Bao K, Wang P. (2023) In-situ and ultrasensitive detection of mercury (II) ions (Hg^{2+}) using the localized surface plasmon resonance (LSPR) nanosensor and the microfluidic chip. Sensors Actuators A Phys., 349: 114074. doi: https://doi.org/10.1016/j.sna.2022.114074

[3] Morsin M, Salleh M. M, Umar A. A, Sahdan M. Z. (2017) Gold nanoplates for a localized surface plasmon resonance-based boric acid sensor. Sensors (Switzerland), 17: 1–9. doi: 10.3390/s17050947

[4] Sun L. L, Leo Y. S, Zhou X, Ng W, Wong T. I, Deng J. (2020) Localized surface plasmon resonance based point-of-care system for sepsis diagnosis. Mater. Sci. Energy Technol., 3: 274–281. doi: 10.1016/j.mset.2019.10.007

[5] Nafisah S, Morsin M, Jumadi N. A, Nayan N, Shah N. S. M, Razali N. L, An'Nisa N. Z. (2020) Improved sensitivity and selectivity of direct localized surface plasmon resonance sensor using gold nanobipyramids for glyphosate detection. IEEE Sens. J., 20: 2378–2389. doi: 10.1109/JSEN.2019.2953928

[6] Bhardwaj H, Sumana G, Marquette C. A. (2021) Gold nanobipyramids integrated ultrasensitive optical and electrochemical biosensor for Aflatoxin B1 detection. Talanta, 222: 121578. doi: 10.1016/j.talanta.2020.121578

[7] Cheng J, Wang X, Nie T, Yin L, Wang S, Zhao Y, Wu H, Mei H. (2020) A novel electrochemical sensing platform for detection of dopamine based on gold nanobipyramid/multi-walled carbon nanotube hybrids. Anal. Bioanal. Chem., 412: 2433–2441. doi: 10.1007/s00216-020-02455-5

[8] Oo A. M, Al-abed A. A, Lwin O. M, Kanneppady S. S, Sim T. Y, Mukti N. A, Zahariluddin A. S, Jaffar F. (2020) Type 2 diabetes mellitus prediction in Malaysia using modified diabetes risk assessment tool. Malaysian J. Public Heal. Med., 20: 15–21, doi: 10.37268/mjphm/vol.20/no.1/art.442

[9] Saeedi P, Petersohn I, Salpea P, Malanda B, Karuranga S, Unwin N, Colagiuri S, Guariguata L, Motala A. A, Ogurtsova K. (2019) Global and regional diabetes prevalence estimates for 2019 and projections for 2030 and 2045: Results from the International Diabetes Federation Diabetes Atlas. Diabetes Res. Clin. Pract., 157: 107843. doi: 10.1016/j.diabres.2019.107843

[10] Ganasegeran K, Hor C. P, Jamil M. F. A, Loh H. C, Noor J. M, Hamid N. A, Suppiah P. D, Manaf M. R. A, Ch'ng A. S. H, Looi I. (2020) A systematic review of the economic burden of type 2 diabetes in Malaysia. Int. J. Environ. Res. Public Health, 17: 1–23. doi: 10.3390/ijerph17165723

[11] Chen J, Yan J, Dou B, Feng Q, Miao X, Wang P. (2021) Aggregatable thiol-functionalized carbon dots-based fluorescence strategy for highly sensitive detection of glucose based on target-initiated catalytic oxidation. Sensors Actuators B Chem., 330: 129325, doi: 10.1016/j.snb.2020.129325

[12] Samanta A, Dhar B. B, Devi R. N. (2012) Novel porous silica encapsulated Au nanoreactors as peroxidase mimic for one-pot glucose detection. New J. Chem., 36: 2625–2629, doi: 10.1039/c2nj40665a

[13] Akhtar M. A, Batool R, Hayat A, Han D, Riaz S, Khan S. U, Nasir M, Nawaz M. H, Niu L. (2019) Functionalized graphene oxide bridging between enzyme and au-sputtered screen-printed interface for glucose detection. ACS Appl. Nano Mater., 2: 1589–1596. doi: 10.1021/acsanm.9b00041

[14] Chu Z, Liu Y, Xu Y, Shi L, Peng J, Jin W. (2015) In-situ fabrication of well-distributed gold nanocubes on thiol graphene as a third-generation biosensor for ultrasensitive glucose detection. Electrochim. Acta, 176: 162–171. doi: 10.1016/j.electacta.2015.06.123

[15] Forlenza G. P, Buckingham B. A, Brown S. A, Bode B. W, Levy C. J, Criego A. B, Wadwa R. P, Cobry E. C, Slover R. J. (2021) First outpatient evaluation of a tubeless automated insulin delivery system with customizable glucose targets in children and adults with type 1 diabetes. Diabetes Technol. Ther., 23: 410–424. doi: 10.1089/dia.2020.0546

[16] An'Nisa N. Z, Morsin M, Sanudin R, Razali N. L, Nafisah S. (2020) Controlled wet chemical synthesis of gold nanorods for triclopyr butotyl herbicide detection based-plasmonic sensor. Sens. Bio-Sensing Res., 29: 100359. doi: 10.1016/j.sbsr.2020.100359

[17] Nafisah S, Morsin M, Sanudin R, Nayan N, Yusop M. Z. M, Razali N. L, Shah N. Z. A. M. (2021) Effect of additive acid on seeded growth of gold nanobipyramids. J. Phys. Chem. Solids, 148: 109764. doi: 10.1016/j.jpcs.2020.109764

[18] Shah N. Z. A. M, Morsin M, Sanudin R, Razali N. L, Nafisah S, Soon C. F. (2020) Effects of growth solutions ageing time to the formation of gold nanorods via two-step approach for plasmonic applications. Plasmonics, 15: 923–932. doi: 10.1007/s11468-019-01098-2

[19] Capek I. (2013) Preparation and functionalization of gold nanoparticles. J. Surf. Sci. Technol, 29: 1–18.

[20] Chang Y, Wang L, Li R, Zhang Z, Wang Q, Yang J, Guo C. F, Pan T. (2021) First decade of interfacial iontronic sensing: from droplet sensors to artificial skins. Adv. Mater., 33: 2003464. doi: 10.1002/adma.202003464

[21] Lin L, Weng S, Zheng Y, Liu X, Ying S, Chen F, You D. (2020) Bimetallic PtAu alloy nanomaterials for nonenzymatic selective glucose sensing at low potential. J. Electroanal. Chem., 865: 114147. doi: 10.1016/j.jelechem.2020.114147